

pubs.acs.org/JPCB Article

Temperature-Dependent Fluorescence of mPlum Fluorescent Protein from 295 to 20 K

Taecheon Lyu, So Hyeong Sohn, Ralph Jimenez,* and Taiha Joo*



Cite This: J. Phys. Chem. B 2022, 126, 2337-2344



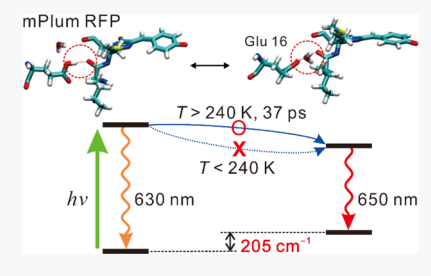
ACCESS I

Metrics & More



SI Supporting Information

ABSTRACT: The development of bright fluorescent proteins (FPs) emitting beyond 600 nm continues to be of interest both from a fundamental perspective in understanding protein-chromophore interactions and from a practical perspective as these FPs would be valuable for cellular imaging. We previously reported ultrafast spectral observations of the excited-state dynamics in mPlum resulting from interconversion between direct hydrogen bonding and water-mediated hydrogen bonding between the chromophore acylimine carbonyl and the Glu16 side chain. Here, we report temperature-dependent steady-state and time-resolved fluorescence measurements of mPlum and its E16H variant, which does not contain a side-chain permitting hydrogen bonding with the acylimine carbonyl.



Lowering the temperature of the system freezes interconversion between the hydrogen-bonding states, thus revealing the spectral signatures of the two states. Analysis of the temperature-dependent spectra assuming Boltzmann populations of the two states yields a 205 cm⁻¹ energy difference. This value agrees with the predictions from a quantum mechanics/molecular mechanics study of mPlum (198 cm⁻¹). This study demonstrates the first use of cryogenic spectroscopy to quantify the energetics and timescales of FP chromophore structural states that were only previously obtained from computational methods and further confirms the importance of acylimine hydrogen-bonding dynamics to the fluorescence spectral shifts of red FPs.

1. INTRODUCTION

The discovery of fluorescent proteins (FPs) in the 1960s, their heterologous expression in the 1990s, and their subsequent development into a diverse color palette has revolutionized biological research by allowing the visualization of an immense range of cellular dynamics including gene expression, protein localization and trafficking down to the single molecule and sub-diffraction-limited spatial regime, and protein-protein interaction. 1-5 The chromophore of an FP is formed by an autocatalytic reaction from the expressed polypeptide sequence, which together with numerous protein interactions determines the photophysical characteristics of the FP such as absorption and fluorescence spectra, brightness, and photostability. Red fluorescent proteins (RFPs) are particularly useful as markers for live cell imaging because hemoglobin and other endogenous chromophores in mammalian tissues strongly absorb light at wavelengths below 600 nm.^{3,7,8} However, there remains a lack of fluorophores available in the far-red region (fluorescence beyond 600 nm). Since most red-shifted emitting RFPs have quantum yields lower than widely used green FPs (GFPs), a substantial amount of research has focused on improving their performance. 9-12 Studies of the excited-state dynamics can provide insight to guide the development of new RFPs by revealing the structural factors involved in the Stokes shift and nonradiative processes.

In general, the complex structure and dynamics of proteins lead to a combination of spectral congestion and molecular motions over many orders of magnitude in time, which makes it difficult to clearly assign their excited-state processes with either frequency- or time-resolved spectroscopy. Many studies rely on theoretical calculations for the interpretation of excited-state processes, 13-21 but this is challenging due to the limitations in the accuracy and range of timescales accessible to quantum mechanical (QM) calculations on such large systems. Low-temperature fluorescence spectroscopy is one approach for simplifying the dynamics of complex systems. Fluorescence spectroscopy exclusively observes excited-state processes, providing an advantage over absorption-based spectroscopies which probe an amalgam of the ground- and excited-state dynamics that are usually difficult to disentangle. At low temperatures, the conformational space can be reduced by narrowing the Boltzmann distribution, potentially allowing the observation of specific conformational structures. Furthermore, thermally activated nuclear motions are slower, which facilitates a clearer observation of dynamics. The motion of water molecules is restricted below its freezing temperature, thereby greatly limiting the rate of reactions involving water (e.g., solvation and water-mediated hydrogen bonding). In particular, dynamical transition of biological macromolecules at

Received: December 13, 2021 Revised: March 7, 2022 Published: March 17, 2022





around 220 K has been observed, and its origin has been the subject of intense discussion. $^{22-30}$

The DsRed family of proteins, which are RFPs derived from Discosoma striata, share a common chromophore including a long π -conjugated system, extended by an N-acylimine group leading to a red-shifted fluorescence compared to GFPs. Like all RFPs, the chromophores within the DsRed family are stabilized by multiple interactions with the surrounding amino acids, which affect the flexibility and homogeneity of its structure. The mPlum RFP shows the largest Stokes shift (59 nm) in this family (Figure 1). Experimental and

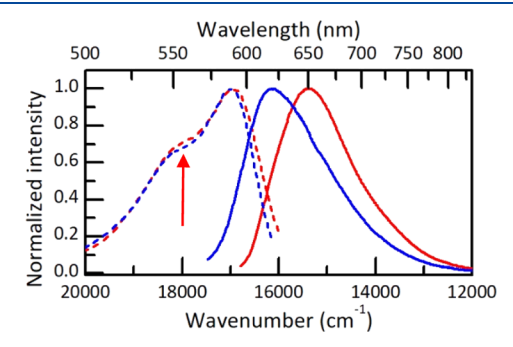


Figure 1. Excitation (dashed lines) and fluorescence (solid lines) spectra of mPlum (red) and E16H mutant (blue) at room temperature. For the excitation spectra, the fluorescence was detected at the maximum intensity of each spectrum. The excitation wavelength (555 nm) of the fluorescence spectra is indicated by the red arrow.

theoretical investigations of mPlum support the existence of two distinct conformations of the chromophore to side-chain hydrogen-bonding interactions, involving the acylimine carbonyl group, in the electronic ground state. These conformations shown in Figure 2 are distinguished as direct

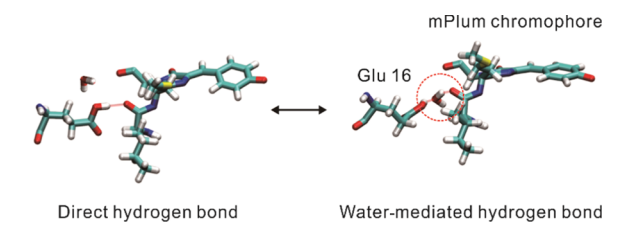


Figure 2. Two conformations of mPlum distinguished as DHB and WMHB interactions between the Glu16 side chain and the chromophore acylimine carbonyl oxygen. The water molecule inside the red circle mediates the hydrogen bonding (mPlum PDB code: 2QLG).

In this study, time-resolved and steady-state fluorescence spectroscopies at cryogenic temperatures were performed using a closed-cycle cryostat with liquid helium. We analyzed the temperature-dependent fluorescence spectra using the Boltzmann distribution and identified the spectral characteristics of the two conformers. Temperature dependence of the energy levels and populations of the two conformers were resolved with steady-state spectroscopy, while the interconversion dynamics was measured with TF spectroscopy.

2. MATERIALS AND METHODS

We used previously reported methods²¹ to prepare mPlum and its E16H mutant, which lacks the acylimine hydrogen bond donor from position 16, dissolved in a pH 8.0 Tris buffer. For low-temperature experiments, a continuous flow liquid helium cryostat (Janis, ST-100) was used in the temperature range 20–295 K with an interval of 10 K. The sample (\sim 200 μ M) was loaded between uncoated fused silica plates of 100 μm beam pathlength to obtain good thermal contact.³⁶ For a full set of measurements, temperature was first lowered to 20 K and maintained for a long time (>3 h) until two fluorescence spectra taken in 1 h interval show no change. The spectra were measured while increasing the temperature in 10 K step size with a waiting time of 15 min at each temperature, which was enough to reach equilibrium as verified by the waiting time dependence (Figure S1). The buffer solution with protein becomes opaque when it was frozen. The stationary fluorescence and TF spectra were measured in opaque state without adding any cryoprotectants to avoid any possible alteration of the sample.

The light source was a home-built cavity-dumped femtosecond optical parametric oscillator based on a periodically poled stoichiometric lithium tantalate crystal.³⁵ An excitation wavelength of 555 nm was used for both mPlum and the E16H variant because their excitation spectra are quite similar as shown in Figure 1. The excitation pulses at 555 nm were obtained by the second harmonic generation of the fundamental light (1110 nm, 1 MHz, 40 fs) with a 2 mm thick lithium triborate crystal. The excitation pulse energy was 0.5 nJ, and the excitation beam was loosely focused to a diameter of 1 mm to prevent photodamage. The excitation spectra were measured before and after the experiment to check photodamage (Figure S2). In addition, the TF spectra at room temperature were measured before and after the full temperature cycle (Figure S3) to ensure that the sample is intact. The polarization of the excitation pulse was set at the magic angle (54.7°) with respect to the detection axis to eliminate the effect of reorientational dynamics on the measurement. The fluorescence signal was collected by a 25.4 mm parabolic mirror and dispersed using a monochromator (Acton Research, SP-300) with a 150 grooves/mm grating. The steady-state fluorescence spectra were detected using a charge-coupled device (Andor, DV 420). The TF spectra were measured by the time-correlated single photon counting (TCSPC) method. A hybrid photodetector (HPM100-07, Becker and Hickl GmbH) was used as a detector for the TCSPC, and the instrumental response function of the TCSPC setup was 80 ps [(fwhm) full width at half-maximum].

3. RESULTS AND DISCUSSION

3.1. Temperature-Dependent Steady-State Spectra. Steady-state fluorescence and excitation spectra of mPlum and the E16H variant are shown in Figure 1. Although the

fluorescence maximum of mPlum is red-shifted by 30 nm from that of its E16H mutant at 620 nm, their excitation spectra are quite similar. The additional 30 nm red shift of mPlum was accounted for mainly by the conformational change from the DHB to WMHB form in the excited state. Temperature-dependent steady-state fluorescence spectra of mPlum and the E16H mutant following photoexcitation at 555 nm for both RFPs, normalized by their intensity or integrated area at each temperature, are shown in Figure 3. The fluorescence spectral

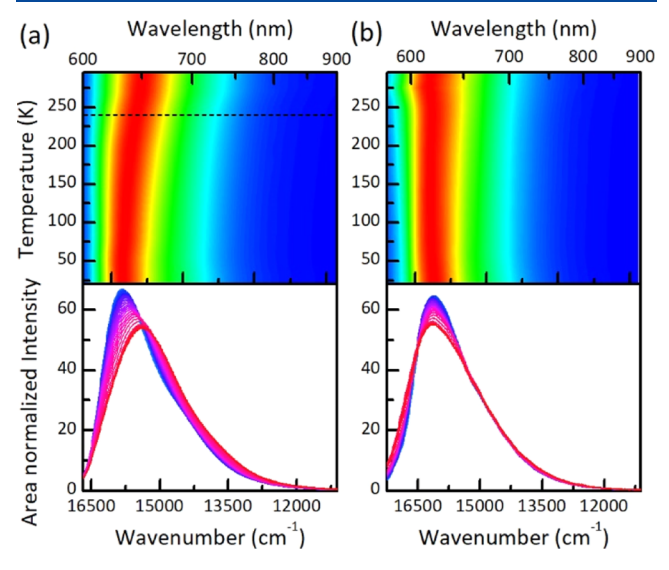


Figure 3. Temperature-dependent steady-state fluorescence spectra of (a) mPlum and (b) E16H variant. The spectrum at each temperature is normalized to the maximum intensity in the top contour plots, and it is normalized to the integrated intensity in the bottom. The dashed line in (a) is 240 K, below which the conformational change from DHB to WMHB is blocked. The EAS analysis used the data below 240 K. In the bottom, the temperature decreases from 295 K (red) to 20 K (blue) by 10 K decrement.

widths of both RFPs narrow as the temperature decreases. The first moments of the fluorescence spectra as a function of temperature (Figure S4 in the Supporting Information) show that mPlum exhibits a spectral blue shift of 300 cm⁻¹ as the temperature decreases from 295 to 50 K, whereas the E16H mutant exhibits a blue shift of less than 50 cm⁻¹ down to 100 K and then a $50\ cm^{-1}$ red shift as the temperature is further lowered. Interestingly, the area-normalized fluorescence spectra of mPlum as a function of temperature show an isoemissive point at 15,400 cm⁻¹ (Figure S5) in the temperature range 240-80 K.³⁷ Although spectral analysis based on the isoemissive point was originally proposed for time-resolved area-normalized emission spectra,³⁷ it can be applied to more general circumstances. When the fluorescence spectra at different temperatures consist of two emitters, an isoemissive point should also be observed, provided the spectrum of each component is invariant upon temperature change. The spectral shifts and observation of the clear isoemissive point strongly suggest that mPlum exists as two emissive forms with temperature-dependent populations, whereas the E16H variant exists as a single emitting form at all temperatures.

As reported previously, 11 mPlum forms a DHB or WMHB between the Glu16 side chain and N-acylimine of the chromophore. Below the freezing point of the aqueous buffer, the transition from the DHB to WMHB form is unfavorable

because water molecules cannot move freely in the solid phase. In fact, dynamical transition of biological macromolecules at around 220 K has been observed, and it was reported that water molecules close to the protein exhibit two distinct relaxations. Therefore, the fluorescence spectra below $\sim\!240$ K may represent the ground-state populations of the two forms without the transition from DHB to WMHB form in the S_1 state because the transition does not occur or occurs slowly compared to the fluorescence lifetime. In contrast, the fluorescence spectrum of the E16H mutant hardly changes with temperature because it exists as a single emitting form.

The temperature-dependent steady-state spectra in Figure 3 were analyzed by global analyses in two different ways; a global analysis based on exponential fits with respect to 1/T, which provides decay associated spectra (DAS) and a model nonlinear least square fit. For the former, it is assumed that the fluorescence intensity (i.e., population) of each species is determined solely by the Boltzmann distribution in the ground state and that the spectral shape of each form is independent of temperature. The fluorescence spectra below 240 K were used because the dynamics from DHB to WMHB form affects the fluorescence intensity at higher temperatures. The fluorescence spectrum at a given temperature is the sum of the spectrum of each species weighted by a Boltzmann factor

$$I(\omega, T) = \sum_{i} A_{i}(\omega) \exp[-\Delta E_{i}/kT]$$
(1)

where $A_i(\omega)$ is the fluorescence spectrum of a *i*-th species. In an analogy to the global analysis of time-resolved spectra, the temperature-dependent spectra can be fitted globally by taking 1/T as an independent variable. The global analysis in this way gives the fluorescence spectra associated with constants $k/\Delta E$, which we call the energy-associated spectra (EAS) and the temperature constant, respectively.

The temperature-dependent steady-state fluorescence spectra of mPlum can be fitted well by two EAS shown in Figure 4. The integrated fluorescence intensity changes significantly with temperature because transmission, reflection, and scattering from the sample vary as the temperature is lowered. The areanormalized fluorescence spectra were used to attain the energy dependence while excluding temperature dependence of the

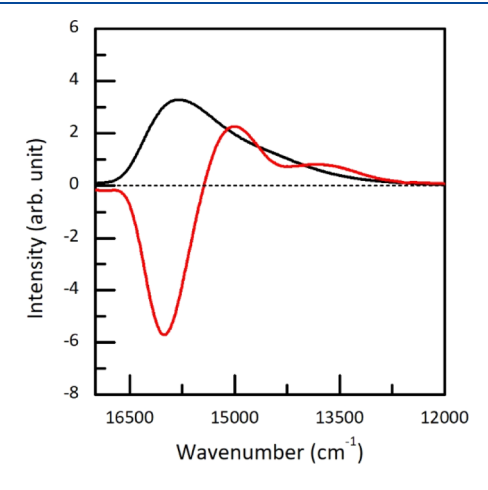


Figure 4. EAS of mPlum obtained from the global fit of the temperature-dependent fluorescence spectra. The temperature constants of the black and red lines are 3.0 and $0.00217~{\rm K}^{-1}$, respectively.

integrated intensity. The EAS with a temperature constant of 3.0 K^{-1} (black line) represents the spectrum in the lowtemperature limit. Because the spectra are normalized for this analysis, the temperature constant should be a large value (infinity) for an ideal two emitter case. The EAS with a temperature constant of 0.00217 K⁻¹, which corresponds to the energy difference of 319 cm⁻¹, shows a positive (negative) contribution at the low (high) energy side of the fluorescence spectrum. That is, the EAS (0.00217 K⁻¹) denotes increase of the high energy side of the spectrum and decrease of the low energy side of the spectrum as the temperature decreases (increase of 1/T). Therefore, the lower energy species (DHB) in the ground state, whose population increases at lower temperatures, emits at higher frequency than the higher energy species (WMHB), and the energy difference between the two species in the ground state is 319 cm⁻¹, which is in reasonable agreement with the value of 198 cm⁻¹ determined previously by quantum mechanics/molecular mechanics (QM/MM) simulation. 19

Although the above global analysis is unbiased as no explicit model is assumed, the temperature dependence of each fluorescence spectrum cannot be incorporated. Thus, we fitted globally the temperature-dependent steady-state spectra of mPlum with two model functions that represent the DHB and WMHB forms. The global analysis was first performed on the E16H mutant in which only one emissive form exists. To accommodate the vibronic structure, which can be more clearly discerned at low temperatures, two lognormal functions are used. A lognormal function is

$$I(\nu; A, \nu_0, \Delta, \gamma) = A \exp \left[-\ln(2) \cdot \left\{ \frac{1}{\gamma} \ln \left(1 + \frac{2\gamma(\nu - \nu_0)}{\Delta} \right) \right\}^2 \right]$$
(2)

where A is the maximum intensity, ν_0 is the peak position, Δ is the width parameter, and γ is the asymmetry parameter. The full width at half-maximum (fwhm) is $\Delta \cdot \sinh(\gamma)/\gamma$. Consequently, four lognormal functions are required to properly fit the fluorescence spectra of mPlum where two emitting species are present. The nonlinear least square fits were performed using the Marquardt algorithm, and we applied a series of constraints during the fits to make the nonlinear least square fits robust. The energy gap of the two vibronic bands, the ratio of the integrated area of the two vibronic bands, and the asymmetry parameters of each band were fixed. The asymmetry parameters were obtained from the fits of the fluorescence spectrum at room temperature. The fwhm of each band is assumed to decay exponentially with 1/T to reflect the narrowing of the width as the temperature decreases.

Global fit results at a few representative temperatures are shown in Figure 5 (see Figures S6 and S7 for other temperatures), and the peak positions and widths versus 1/T are shown in Figure 6. The peak positions of the two vibronic bands of the E16H mutant are invariant with the temperature change, although their widths narrow significantly. Surprisingly, however, the peak positions of mPlum are also practically invariant with the temperature change, even though the fluorescence spectrum of mPlum changes significantly with temperature. This is a strong indication that the temperature dependence of the mPlum arises largely from the change of the

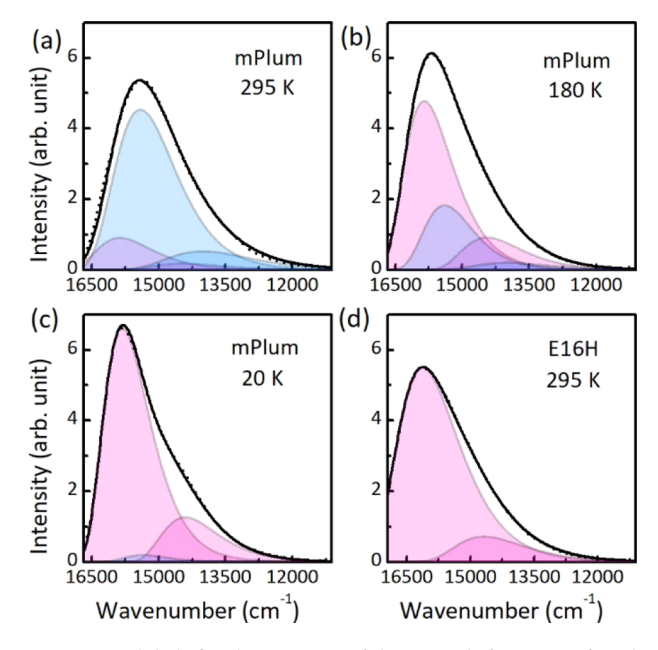


Figure 5. Global fits by a sum of lognormal functions for the temperature-dependent fluorescence spectra of (a-c) mPlum at 295, 180, and 20 K and (d) E16H mutant at 295 K. In the global fits, each chemical species is represented by two lognormal functions because of the vibrational progression. For mPlum, the pink and blue colors represent the fluorescence of the DHB and WMHB forms, respectively.

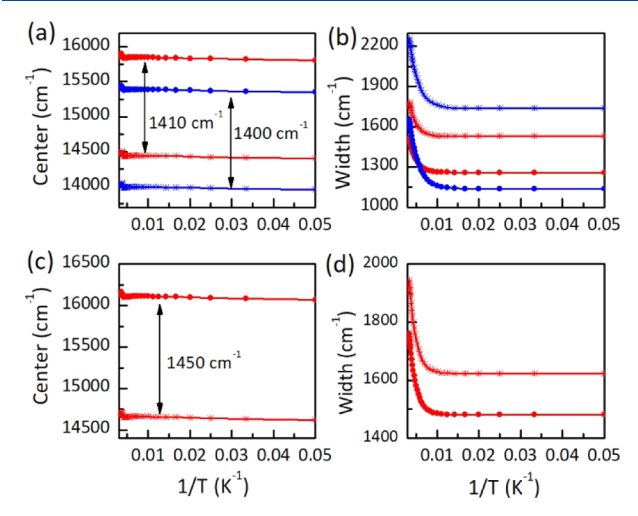


Figure 6. (a,c) Center frequencies and (b,d) widths of the lognormal functions for (a,b) mPlum and (c,d) E16H variant obtained from the global fits in Figure 4. For mPlum, the red and blue colors correspond to the DHB and WMHB forms, respectively. Filled circles and stars are the data corresponding to the high- and low-frequency components of the vibrational progression, respectively, and the lines are guide for the eye.

equilibrium between the DHB and WMHB forms. For the E16H mutant, the fluorescence band peaks at 16110 cm⁻¹, and the energy difference between the two vibrational bands is 1450 cm⁻¹ at all temperatures. For mPlum, the fluorescence bands corresponding to the DHB and WMHB forms peak at 15,850 and 14,440 cm⁻¹, respectively. The vibrational sidebands appear at 1410 and 1400 cm⁻¹ below and match well with that of the E16H mutant. These vibrational progressions are likely to originate from the carbon–carbon

double bond stretching modes as the C=C stretching modes in polyenes and aromatic molecules are around 1400–1600 cm⁻¹. ^{39,40} The spectral widths narrow by about 300 cm⁻¹ for the E16H mutant and the DHB form of mPlum, while they narrow by about 500 cm⁻¹ for the WMHB form of mPlum as the temperature decreases from 295 to 20 K. The larger decrease of the spectral width of WMHB is expected because of its more flexible structure leading to larger inhomogeneity at room temperature.

The integrated intensities of the two bands of mPlum are shown in Figure 7. Because the dynamics from the DHB to

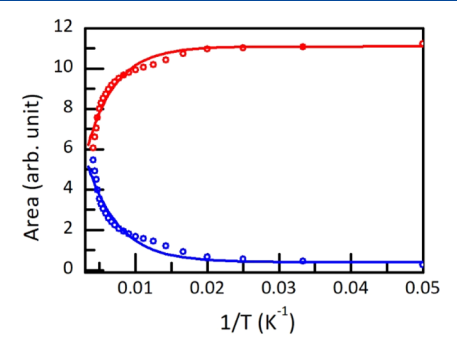
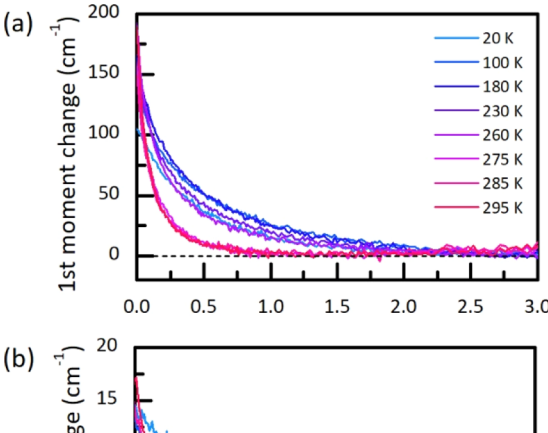


Figure 7. Fluorescence band areas of the DHB (red) and WMHB (blue) forms obtained from the global fits of mPlum in Figure 4 at the temperature range of 20-240 K. The lines are the single exponential fits versus 1/T, which gives a temperature constant of 0.00338 K⁻¹ (205 cm⁻¹).

WMHB form occurs slower than the measurement time window below 240 K (vide infra), the area of the fluorescence spectrum represents the ground--state population in this temperature range. By assuming a Boltzmann distribution of the two conformer populations, an exponential fit versus 1/T gives the energy difference of 205 cm $^{-1}$, which matches well with the previous report (198 cm $^{-1}$). Together with the invariance of the peak position versus temperature, this corroborates our conclusion that mPlum exists as two forms, DHB and WMHB, subject to the equilibrium in the ground state, and transition from DHB to WMHB occurs in the S_1 state at temperatures above \sim 240 K.

The unbiased fitting using EAS analysis gives 318 cm⁻¹ as the energy gap between the two forms, while the log—normal function fit gives 205 cm⁻¹. Although the latter matches better with the previous reported theoretical calculation, both analyses can be regarded to show good agreement with theory, considering uncertainty of the QM/MM calculation results.

3.2. Time-Resolved Fluorescence Spectra. The temperature-dependent TF spectra of mPlum may provide a detailed dynamical information at low temperature. The TF spectra of mPlum and its E16H mutant at several temperatures are shown in the Supporting Information (Figures S8 and S9). Figure 8 shows the first and second moments, which represent the average frequency and width of a spectrum, respectively, of the TF spectra of mPlum at several temperatures. The first moments decrease with time at all temperatures indicating red shifts of the fluorescence spectra with time. In particular, the red shift is accelerated abruptly at 275 K and above. Time constants from single-exponential fits of the first moments are given in Table 1. Correspondingly, the second moments also decrease with time at all temperatures, though by a very small



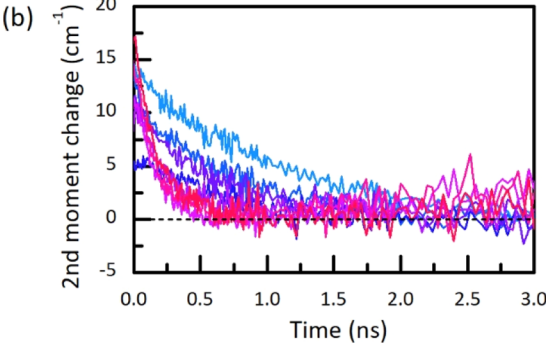


Figure 8. Variations of the (a) first moment and (b) second moment of the TF spectra vs time for mPlum at a few representative temperatures.

magnitude, and the decrease is accelerated at temperatures above 275 K.

Table 1. Time Constants of the First Moments (τ_{fm}) and the DAS $(\tau_1$ and $\tau_2)$ of the TF spectra of mPlum

temp. (K)	295	285	275	260	230	180	100	20
$\tau_{\rm fm}~({ m ps})$	110	140	150	320	420	450	470	450
τ_1 (ps)	70	70	80	130	160	240	260	320
τ_2 (ps)	800	830	860	880	970	1130	1290	1300

The global analysis of the TF spectra at each temperature gives two DAS, with 70–320 and 800–1300 ps time constants. The DAS at a few representative temperatures are shown in Figure 9, and their time constants are listed in Table 1. The slow component should correspond to the fluorescence lifetime of mPlum. Because mPlum exists mostly as the DHB form at 20 K, the 1.3 ns time constant is the lifetime of the DHB form at 20 K. Analogously, the 800 ps time constant at room temperature, which is similar to the value reported previously by the fluorescence up-conversion experiment (610 ps), 11 represents the lifetime of the WMHB form at room temperature. The two fluorescence bands are not distinguishable by the global fitting because of their similar lifetimes. The fast component should reflect the red shift of the fluorescence spectrum as a function of time; positive (decay) amplitude at high-frequency and negative (rise) amplitude at low-frequency regions. In fact, temperature dependences of the time constants of the first moment (Figure 8a) and the fast component parallel each other. In our previous report where the femtosecond fluorescence upconversion method was employed to record the TF spectra, the time constant for the transition from DHB to WMHB at room temperature was determined to be 37 ps. 11 Due to the lower time resolution

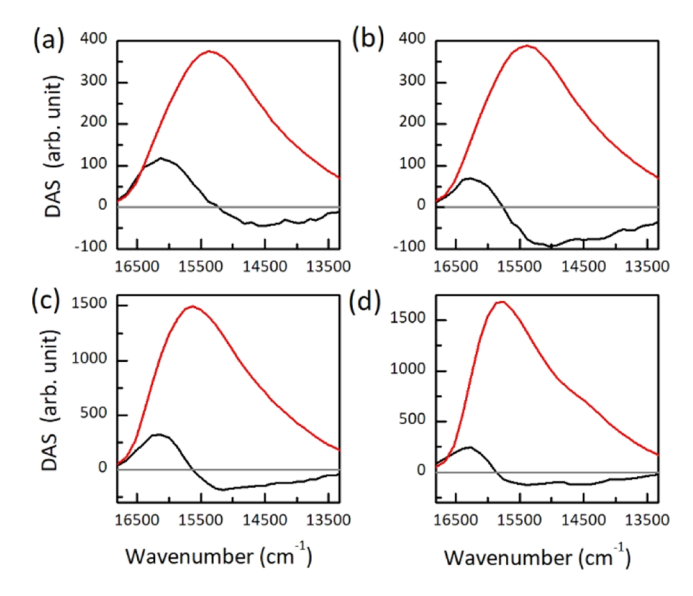


Figure 9. DAS from the global analysis of the TF spectra of mPlum at (a) 295, (b) 275, (c) 180, and (d) 20 K. The time constants of the DAS are listed in Table 1.

(~80 ps) of the current work, the dynamics are only partially resolved at 295 K.

Because the WMHB form emits at a lower frequency, the transition from DHB to WMHB should give rise to a red shift of the spectrum. In addition, the transition should be decelerated at lower temperatures because the motion of water molecules should be suppressed. Considering the temperature dependence of the time constants, it is tempting to assign the fast component of the DAS as the transition time from the DHB to WMHB form. Based on the observations described below, however, we concluded that above ~240 K, the fast component arises mostly from the transition from DHB to WMHB, and below 240 K, it reflects dynamic Stokes shift due to relaxation processes including vibration relaxation and motions of slow solvent and protein backbone.

If the spectral red shift below 240 K originates from the DHB to WMHB transition, the fluorescence of WMHB form should be observed at times longer than the transition time in the TF spectra. However, the slow DAS at temperatures below 240 K is blue-shifted compared to those at higher temperatures appearing near the fluorescence of the DHB form. Note that the DHB form is dominant at low temperatures. The TF spectra at long times (Figure S8) also clearly show this blue shift below ~240 K. The time constants of the DAS (Figure S10) and the first moment (Figure S11) of the TF spectra of mPlum hardly change regardless of the excitation wavelength at all temperatures, which is consistent with the conclusion that the fast DAS cannot be accounted for by the DHB to WMHB transition. The invariance of the TF spectra under the excitation wavelength also indicates that the absorption spectra of the two forms are very similar. The DHB to WMHB transition is expected to be fast above the freezing temperature, to occur slowly in the 240-273 K regime, and to be blocked within the measurement time window at temperatures below 240 K. In the temperature-dependent experiment, there was a waiting time of 15 min for the temperature drop of every 10 K until the spectrum does not change. During this time, the equilibrium between the two forms is established although the sample is frozen. The water molecules inside the protein are

somewhat mobile and can cause slow structural change even at temperatures below the freezing point.²⁹

A notable feature in the TF spectra is that the first and second moments increase past 1 ns at temperatures above 273 K. Because the time constant is longer than the lifetimes of the DHB and WMHB forms, we assume an additional groundstate conformation that has a longer lifetime. We performed a global analysis using >500 ps data to investigate this possibility (Figure S12). An additional slower 1.5 ns DAS that is blueshifted by 110 cm⁻¹ from the slow DAS is obtained, whose contribution is less than 5%. Although the fluorescence intensity and ratio are too small for further analysis, several possibilities can be suggested for this species. The band was observed only above 273 K when the fluorescence of the main component almost disappeared after several nanoseconds. If the species is assumed to exist in the ground state, the energy level should be much higher than DHB and WMHB species, and the spectrum appears several nanoseconds later due to the long lifetime of 1.5 ns. The energy of this long-lifetime species is estimated to lie ~600 cm⁻¹ above the DHB form from the band areas if the Boltzmann distribution is assumed in the ground state. Another possibility is that it may also be originated from structure-changing dynamics in the excited state arising from the WMHB form. The dynamics occurs only above the melting temperature, which indicates that the dynamics is related to the mobility of protein, the motion of hydrogen atom, or isomerization.

For the analyses in Section 3.1 to be valid, the relative fluorescence intensities of the two forms should represent their populations in the ground state. If the two forms have different temperature-dependent nonradiative decay rates, the analyses may not be accurate. We calculated the average lifetimes using the population ratio obtained by the global analysis (Figure 7), assuming that the lifetime of each conformer is the same at all temperatures. The calculated and measured values (τ_2 of DAS in Table 1) shown in Figure S13 match well indicating that their lifetimes do not vary much as a function of temperature.

4. CONCLUSIONS

Steady-state and time-resolved fluorescence spectroscopy was carried out on an RFP mPlum and its E16H mutant over a wide range of temperature from 295 K down to 20 K. The results provide a new insight on the populations and their dynamics of large and complex molecules such as proteins that have multiple conformational isomers. The energetics of each conformer can be obtained by analyzing the temperature-dependent spectra through the Boltzmann distribution. Spectroscopy and dynamics can be observed more clearly by restricting solvent motion and reducing conformational space at low temperatures.

Combined with the result reported previously (ref 11), the conclusions of this work can be summarized with a schematic in Figure 10. There are two major forms of mPlum, DHB, and WMHB forms. Upon photoexcitation, the transition from DHB to WMHB in the S_1 state occurs in 37 ps at room temperature, which is the major aspect contributing to the large Stokes shift of mPlum. The transition, however, is blocked at temperatures below 240 K, and therefore fluorescence spectrum reflects the populations of the two forms in the ground state determined by the Boltzmann distribution. The energy difference between the two forms in the ground state determined by the temperature-dependent steady-state fluorescence spectra is 205 cm $^{-1}$. At 20 K, mPlum

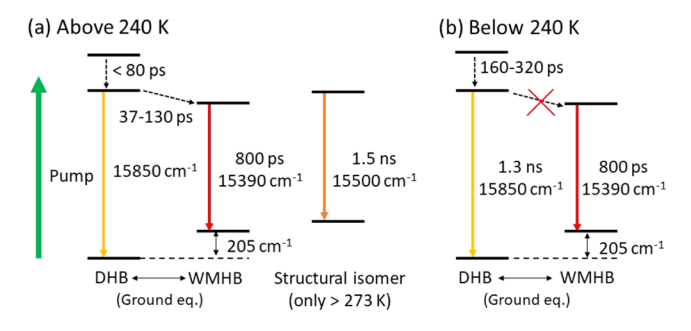


Figure 10. Schematic energy level diagram for photophysics of mPlum at (a) room temperature and (b) temperatures below 240 K. The result from the previous work (ref 11) is combined to produce the schematics. The conformational change is blocked at temperatures below \sim 240 K, and the temperature-dependent population of each form is determined by the Boltzmann distribution in the ground state.

exists as the DHB form almost exclusively, which has a lifetime of 1.3 ns. In addition to the two major forms, a minor (<5%) emissive state having a lifetime of 1.5 ns is observed. This species can be a structural isomer, or it could be a reaction product in the excited state arising from the WMHB form as it is observed only above the melting temperature.

ASSOCIATED CONTENT

Supporting Information

The Supporting Information is available free of charge at https://pubs.acs.org/doi/10.1021/acs.jpcb.1c10516.

First moments of the fluorescence spectra versus temperature, isoemissive point versus temperature, global fit results, temperature-dependent TF spectra, excitation wavelength dependence of DAS, excitation wavelength-dependent first moment of TF spectra, and DAS of lone time TF spectra (PDF)

AUTHOR INFORMATION

Corresponding Authors

Ralph Jimenez — JILA, University of Colorado, and NIST, Boulder, Colorado 80309, United States; Department of Chemistry, University of Colorado, Boulder, Colorado 80309, United States; orcid.org/0000-0002-8989-405X; Email: rjimenez@jila.colorado.edu

Taiha Joo – Department of Chemistry, Pohang University of Science and Technology (POSTECH), Pohang 37673, South Korea; orcid.org/0000-0003-2690-7789; Email: thjoo@postech.ac.kr

Authors

Taecheon Lyu – Department of Chemistry, Pohang University of Science and Technology (POSTECH), Pohang 37673, South Korea

So Hyeong Sohn – Department of Chemistry, Pohang University of Science and Technology (POSTECH), Pohang 37673, South Korea

Complete contact information is available at: https://pubs.acs.org/10.1021/acs.jpcb.1c10516

Notes

The authors declare no competing financial interest.

ACKNOWLEDGMENTS

T.J. acknowledges the support by the National Research Foundation of Korea (NRF) grant funded by the Korea government (MSIT) (nos. 2019R1A2C2010445 and 2020R1A5A1019141). R.J. acknowledges the support by the NSF Physics Frontier Center at JILA (PHY 1734006 to R.J.). We thank Pia Friis for sample preparation. R.J. is a staff member in the Quantum Physics Division of the National Institute of Standards and Technology (NIST). Certain commercial equipment, instruments, or materials are identified in this paper in order to specify the experimental procedure adequately. Such identification is not intended to imply recommendation or endorsement by the NIST nor is it intended to imply that the materials or equipment identified are necessarily the best available for the purpose.

■ REFERENCES

- (1) Chudakov, D. M.; Matz, M. V.; Lukyanov, S.; Lukyanov, K. A. Fluorescent Proteins and Their Applications in Imaging Living Cells and Tissues. *Physiol. Rev.* **2010**, *90*, 1103–1163.
- (2) Mishin, A. S.; Belousov, V. V.; Solntsev, K. M.; Lukyanov, K. A. Novel Uses of Fluorescent Proteins. *Curr. Opin. Chem. Biol.* **2015**, 27, 1–9
- (3) Shu, X.; Royant, A.; Lin, M. Z.; Aguilera, T. A.; Lev-Ram, V.; Steinbach, P. A.; Tsien, R. Y. Mammalian Expression of Infrared Fluorescent Proteins Engineered from a Bacterial Phytochrome. *Science* **2009**, 324, 804–807.
- (4) Wiedenmann, J. r.; Oswald, F.; Nienhaus, G. U. Fluorescent Proteins for Live Cell Imaging: Opportunities, Limitations, and Challenges. *IUBMB Life* **2009**, *61*, 1029–1042.
- (5) Ntziachristos, V. Going Deeper Than Microscopy: the Optical Imaging Frontier in Biology. *Nat. Methods* **2010**, *7*, 603–614.
- (6) Moore, M. M.; Oteng-Pabi, S. K.; Pandelieva, A. T.; Mayo, S. L.; Chica, R. A. Recovery of Red Fluorescent Protein Chromophore Maturation Deficiency through Rational Design. *PLoS One* **2012**, *7*, No. e52463.
- (7) Yang, M.; Jiang, P.; Yamamoto, N.; Li, L.; Geller, J.; Moossa, A. R.; Hoffman, R. M. Real-Time Whole-Body Imaging of an Orthotopic Metastatic Prostate Cancer Model Expressing Red Fluorescent Protein. *Prostate* **2005**, *62*, 374–379.
- (8) Shcherbakova, D. M.; Subach, O. M.; Verkhusha, V. V. Red Fluorescent Proteins: Advanced Imaging Applications and Future Design. *Angew. Chem., Int. Ed.* **2012**, *51*, 10724–10738.
- (9) Merzlyak, E. M.; Goedhart, J.; Shcherbo, D.; Bulina, M. E.; Shcheglov, A. S.; Fradkov, A. F.; Gaintzeva, A.; Lukyanov, K. A.; Lukyanov, S.; Gadella, T. W. J.; et al. Bright Monomeric Red Fluorescent Protein with an Extended Fluorescence Lifetime. *Nat. Methods* 2007, 4, 555.
- (10) Shaner, N. C.; Campbell, R. E.; Steinbach, P. A.; Giepmans, B. N. G.; Palmer, A. E.; Tsien, R. Y. Improved Monomeric Red, Orange and Yellow Fluorescent Proteins Derived from Discosoma Sp. Red Fluorescent Protein. *Nat. Biotechnol.* **2004**, 22, 1567.
- (11) Yoon, E.; Konold, P. E.; Lee, J.; Joo, T.; Jimenez, R. Far-Red Emission of mPlum Fluorescent Protein Results from Excited-State Interconversion between Chromophore Hydrogen-Bonding States. *J. Phys. Chem. Lett.* **2016**, *7*, 2170–2174.
- (12) Konold, P. E.; Yoon, E.; Lee, J.; Allen, S. L.; Chapagain, P. P.; Gerstman, B. S.; Regmi, C. K.; Piatkevich, K. D.; Verkhusha, V. V.; Joo, T.; et al. Fluorescence from Multiple Chromophore Hydrogen-Bonding States in the Far-Red Protein TagRFP675. *J. Phys. Chem. Lett.* 2016, 7, 3046–3051.
- (13) Coppola, F.; Perrella, F.; Petrone, A.; Donati, G.; Rega, N. A Not Obvious Correlation Between the Structure of Green Fluorescent Protein Chromophore Pocket and Hydrogen Bond Dynamics: A Choreography From ab initio Molecular Dynamics. *Front. Mol. Biosci.* **2020**, *7*, 569990.

- (14) Smyrnova, D.; Marín, M. d. C.; Olivucci, M.; Ceulemans, A. Systematic Excited State Studies of Reversibly Switchable Fluorescent Proteins. *J. Chem. Theory Comput.* **2018**, *14*, 3163–3172.
- (15) Pirojsirikul, T.; Götz, A. W.; Weare, J.; Walker, R. C.; Kowalski, K.; Valiev, M. Combined Quantum-Mechanical Molecular Mechanics Calculations with NWChem and AMBER: Excited State Properties of Green Fluorescent Protein Chromophore Analogue in Aqueous Solution. *J. Comput. Chem.* **2017**, *38*, 1631–1639.
- (16) Minezawa, N.; Nakajima, T. Quantum Mechanical/Molecular Mechanical Trajectory Surface Hopping Molecular Dynamics Simulation by Spin-Flip Time-Dependent Density Functional Theory. *J. Chem. Phys.* **2020**, *152*, 024119.
- (17) Ramos, F. C.; Cupellini, L.; Mennucci, B. Computational Investigation of Structural and Spectroscopic Properties of LOV-Based Proteins with Improved Fluorescence. *J. Phys. Chem. B* **2021**, 125, 1768–1777.
- (18) Grigorenko, B. L.; Krylov, A. I.; Nemukhin, A. V. Molecular Modeling Clarifies the Mechanism of Chromophore Maturation in the Green Fluorescent Protein. *J. Am. Chem. Soc.* **2017**, *139*, 10239–10249
- (19) Faraji, S.; Krylov, A. I. On the Nature of an Extended Stokes Shift in the mPlum Fluorescent Protein. *J. Phys. Chem. B* **2015**, *119*, 13052–13062.
- (20) Armengol, P.; Gelabert, R.; Moreno, M.; Lluch, J. M. Chromophore Interactions Leading to Different Absorption Spectra in mNeptunel and mCardinal Red Fluorescent Proteins. *Phys. Chem. Chem. Phys.* **2016**, *18*, 16964–16976.
- (21) Konold, P.; Regmi, C. K.; Chapagain, P. P.; Gerstman, B. S.; Jimenez, R. Hydrogen Bond Flexibility Correlates with Stokes Shift in mPlum Variants. *J. Phys. Chem. B* **2014**, *118*, 2940–2948.
- (22) Chen, S.-H.; Liu, L.; Fratini, E.; Baglioni, P.; Faraone, A.; Mamontov, E. Observation of Fragile-to-Strong Dynamic Crossover in Protein Hydration Water. *Proc. Natl. Acad. Sci.* **2006**, *103*, 9012–9016.
- (23) Roh, J. H.; Curtis, J. E.; Azzam, S.; Novikov, V. N.; Peral, I.; Chowdhuri, Z.; Gregory, R. B.; Sokolov, A. P. Influence of Hydration on the Dynamics of Lysozyme. *Biophys. J.* **2006**, *91*, 2573–2588.
- (24) Parak, F.; Knapp, E. W. A Consistent Picture of Protein Dynamics. *Proc. Natl. Acad. Sci.* **1984**, *81*, 7088–7092.
- (25) Doster, W.; Cusack, S.; Petry, W. Dynamical Transition of Myoglobin Revealed by Inelastic Neutron Scattering. *Nature* **1989**, 337, 754–756.
- (26) Rasmussen, B. F.; Stock, A. M.; Ringe, D.; Petsko, G. A. Crystalline Ribonuclease A Loses Function Below the Dynamical Transition at 220 K. *Nature* **1992**, 357, 423–424.
- (27) Tarek, M.; Tobias, D. J. Role of Protein-Water Hydrogen Bond Dynamics in the Protein Dynamical Transition. *Phys. Rev. Lett.* **2002**, 88, 138101.
- (28) Camisasca, G.; De Marzio, M.; Corradini, D.; Gallo, P. Two Structural Relaxations in Protein Hydration Water and Their Dynamic Crossovers. *J. Chem. Phys.* **2016**, *145*, 044503.
- (29) Magazù, S.; Migliardo, F.; Benedetto, A. Puzzle of Protein Dynamical Transition. *J. Phys. Chem. B* **2011**, *115*, 7736–7743.
- (30) Bin, M.; Yousif, R.; Berkowicz, S.; Das, S.; Schlesinger, D.; Perakis, F. Wide-Angle X-Ray Scattering and Molecular Dynamics Simulations of Supercooled Protein Hydration Water. *Phys. Chem. Chem. Phys.* **2021**, 23, 18308–18313.
- (31) Strack, R. L.; Strongin, D. E.; Mets, L.; Glick, B. S.; Keenan, R. J. Chromophore Formation in DsRed Occurs by a Branched Pathway. *J. Am. Chem. Soc.* **2010**, *132*, 8496–8505.
- (32) Piatkevich, K. D.; Malashkevich, V. N.; Morozova, K. S.; Nemkovich, N. A.; Almo, S. C.; Verkhusha, V. V. Extended Stokes Shift in Fluorescent Proteins: Chromophore—Protein Interactions in a Near-Infrared TagRFP675 Variant. *Sci. Rep.* **2013**, *3*, 1847.
- (33) Abbyad, P.; Childs, W.; Shi, X.; Boxer, S. G. Dynamic Stokes Shift in Green Fluorescent Protein Variants. *Proc. Natl. Acad. Sci.* **2007**, *104*, 20189–20194.

- (34) Wang, L.; Jackson, W. C.; Steinbach, P. A.; Tsien, R. Y. Evolution of New Nonantibody Proteins via Iterative Somatic Hypermutation. *Proc. Natl. Acad. Sci. U.S.A.* **2004**, *101*, 16745.
- (35) Yoon, E.; Joo, T. Cavity-Dumped Femtosecond Optical Parametric Oscillator Based on Periodically Poled Stoichiometric Lithium Tantalate. *Laser Phys. Lett.* **2016**, *13*, 035301.
- (36) Son, J.; Joo, T. Ultrafast Time-Resolved Fluorescence at Cryogenic Temperature. *Rev. Sci. Instrum.* **2018**, *89*, 083115.
- (37) Koti, A. S. R.; Periasamy, N. Application of Time Resolved Area Normalized Emission Spectroscopy to Multicomponent Systems. *J. Chem. Phys.* **2001**, *115*, 7094–7099.
- (38) Marquardt, D. W. An Algorithm for Least-Squares Estimation of Nonlinear Parameters. *J. Soc. Ind. Appl. Math.* **1963**, *11*, 431–441.
- (39) Mustroph, H.; Towns, A. Fine Structure in Electronic Spectra of Cyanine Dyes: Are Sub-Bands Largely Determined by a Dominant Vibration or a Collection of Singly Excited Vibrations? *ChemPhysChem* **2018**, *19*, 1016–1023.
- (40) Fleming, I.; Williams, D. Ultraviolet and Visible Spectra. *Spectroscopic Methods in Organic Chemistry*; Springer International Publishing: Cham, 2019; pp 55–83.

□ Recommended by ACS

Fluorescence Modulation by Ultrafast Chromophore Twisting Events: Developing a Powerful Toolset for Fluorescent-Protein-Based Imaging

Longteng Tang and Chong Fang

DECEMBER 09, 2021

THE JOURNAL OF PHYSICAL CHEMISTRY B

READ 🗹

Characterization of Photophysical Properties of Photoactivatable Fluorescent Proteins for Super-Resolution Microscopy

Antai Tao, Junhua Yuan, et al.

FEBRUARY 17, 2020

THE JOURNAL OF PHYSICAL CHEMISTRY B

READ 🗹

Mechanistic Investigations of Green mEos4b Reveal a Dynamic Long-Lived Dark State

Elke De Zitter, Dominique Bourgeois, et al.

MAY 28, 2020

JOURNAL OF THE AMERICAN CHEMICAL SOCIETY

READ 🗹

Fully Quantum Chemical Treatment of Chromophore-Protein Interactions in Phytochromes

Ronald González and Maria A. Mroginski

NOVEMBER 01, 2019

THE JOURNAL OF PHYSICAL CHEMISTRY B

READ 🗹

Get More Suggestions >